Electronic Structure Reconstruction across the Antiferromagnetic Transition in $TaFe_{1.23}Te_3$ Spin Ladder *

Xu M.(徐敏)[1], Wang Limin(王莉敏)[2], Peng R.(彭瑞)[1,7], Ge Q. Q.(葛青亲)[1], Chen F.(陈飞)[1], Ye Z. R.(叶子荣)[1], Zhang Y.(张焱)[1], Chen S. D.(陈苏迪)[1], Xia M.(夏淼)[1], Liu R. H.(刘荣华)[3], Arita M.[4], Shimada K.[4], Namatame H.[4], Taniguchi M.[4], Matsunami M.[5], Kimura S.[5], Shi M.(史明)[6], Chen X. H.(陈仙辉)[3], Yin Wei-Guo(尹卫国)[2], Ku Wei(顾威)[2],**, Xie B. P.(谢斌平)[1,7**], Feng D. L.(封东来)[1,7**]

[1] *State Key Laboratory of Surface Physics, Department of Physics, and Advanced Materials Laboratory, Fudan University, Shanghai 200433, People's Republic of China*

[2] *Condensed Matter Physics and Materials Science Department, Brookhaven National Laboratory, Upton, New York 11973, USA*

[3] *Hefei National Laboratory for Physical Sciences at Microscale and Department of Physics, University of Science and Technology of China, Hefei, Anhui 230026, China*

[4] *Hiroshima Synchrotron Radiation Center, Hiroshima University, Hiroshima 739-8526, Japan*

[5] *UVSOR Facility, Institute for Molecular Science, Okazaki 444-8585, Japan*

[6] *Swiss Light Source, Paul-Scherrer Institut, 5232 Villigen, Switzerland*

[7] *Collaborative Innovation Center of Advanced Microstructures, 22 Hankou Road, Gulou, Nanjing 210093*

(Received 16 July 2014)

With angle-resolved photoemission spectroscopy, we studied the electronic structure of $TaFe_{1.23}Te_3$, a two-leg spin ladder compound with a novel antiferromagnetic ground state. Quasi-two-dimensional Fermi surface is observed, with sizable inter-ladder hopping. Moreover, instead of observing an energy gap at the Fermi surface in the antiferromagnetic state, we observed the shifts of various bands. Combining these observations with density-functional-theory calculations, we propose that the large scale reconstruction of the electronic structure, caused by the interactions between the coexisting itinerant electrons and local moments, is most likely the driving force of the magnetic transition. Thus $TaFe_{1.23}Te_3$ serves as a simpler platform that contains similar ingredients as the parent compounds of iron-based superconductors.

PACS: 74.25.Jb,74.70.-b,71.20.-b DOI:10.1000/0000-0000/00/0/000000

Several iron-based spin chain/ladder systems have been discovered recently, including $TaFe_{1.23}Te_3$,[1] $BaFe_2Se_3$,[2,3] $Ce_2O_2FeSe_2$,[4] single layer $K_xFe_{2-y}Se_2$ (110) film,[5] and the signature of superconductivity and antiferromagnetic (AFM) order in the alkali-doped FeSe-ladder system resembles the parent compounds of iron-based superconductors.[4,5] Meanwhile, all these materials share a similar structural character: a layered, quasi-one-dimensional structure with edge sharing FeX_4 (X=Te, Se) plaquettes. For example, $TaFe_{1.23}Te_3$ can be viewed as Fe-Fe zig-zag spin ladder compound with adjacent ladders connected by a Ta/Te network as illustrated in Figs. 1(a) and 1(b). It exhibits an AFM order with an unusual ferromagnetic (FM) coupling in the cleavage plane and an antiferromagnetic coupling out of plane as shown in Fig. 1(a), and the local moment of about 2 μ_B/Fe resembles that of FeTe.[6,7] Due to their similarities, these ladder compounds can be considered as low dimensional siblings of the iron-based superconductors. Besides the interests in themselves as iron-based spin ladders, experimental study in combination with readily treatable theoretical modeling of these systems would deepen our understanding of magnetism in iron-based superconductors.

In this letter, we study the electronic structure of $TaFe_{1.23}Te_3$ by angle-resolved photoemission spectroscopy (ARPES) and band calculations. Moreover, we find that features far below the Fermi energy (E_F) shift abruptly across the AFM transition, instead of opening a gap, resembling the electronic structure reconstruction across the AFM transition in 2D iron pnictides.[8−11] Our results suggest that the critical ingredients of the magnetism in the parent compounds of iron-based superconductors, such as local moments and the Hund's rule coupling, together with the double exchange interactions across the in-plane ladders, conspire the novel ground state in $TaFe_{1.23}Te_3$.

Needle-shaped $TaFe_{1.23}Te_3$ single crystals were synthesized by chemical vapor transport method.[1] The resistivity shows metallic behavior and an anomaly at the Neel temperature (T_N) around 160 K,[1] resembling the AFM transition of $BaFe_2As_2$.[12] ARPES measurements were performed at beamline 9A of Hiroshima Synchrotron Radiation Center, the SIS beamline of the Swiss Light Source with Scienta R4000 elec-

*Supported by the National Basic Research Program of China under Grant Nos 2012CB921400, 2011CB921802 and 2011CBA00112.

**Correspondence author. Email: weiku@bnl.gov; dlfeng@fudan.edu.cn

tron analyzers, and BL7 of Ultraviolet Synchrotron Orbital Radiation facility with an MBS A-1 electron analyzer. The overall energy resolution is $\sim$ 15 meV, and angular resolution is $\sim$ 0.3°.

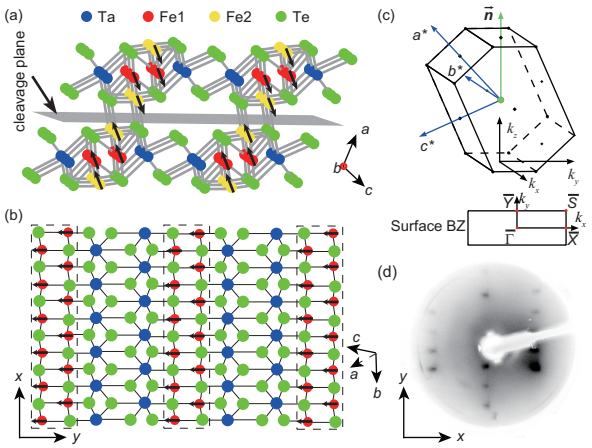

Fig. 1. (Color online). Crystal structure and Brillouin zone (BZ) of $TaFe_{1.23}Te_3$. (a) Schematic illustration of crystal structure and spin structure following neutron scattering result[6]. The Fe2 atoms partially and randomly occupy the interstitial sites. (b) A projection of the ladder structure onto the natural cleavage (-101) plane. The Fe-Fe zig-zag two-leg ladders are encircled by dashed lines. Note that the interstitial Fe2 is not shown here. (c) Three-dimensional BZ of $TaFe_{1.23}Te_3$ with the monoclinic structure. The direction of vector $\vec{n}$ is normal to the cleaved surface (-101) in the reciprocal space. The bottom part gives the surface BZ. Hereafter, we define the $\bar{\Gamma}\bar{X}$ and $\bar{\Gamma}\bar{Y}$ axis to be parallel to and perpendicular to the ladder, respectively. $\bar{\Gamma}\bar{X}$= 0.863 Å^{-1} and $\bar{\Gamma}\bar{Y}$= 0.305 Å^{-1}. (d) The low-energy electron diffraction (LEED) pattern of $TaFe_{1.23}Te_3$ taken at 250 K in the paramagnetic state with 100 eV incident electrons. Note that $\bar{\Gamma}\bar{X}/\bar{\Gamma}\bar{Y}$ $\approx$2.8 is consistence with the LEED pattern.

$TaFe_{1.23}Te_3$ crystalizes in a monoclinic $P2_1/m$ structure with lattice constants a =7.4262 Å, b =3.6374 Å, c = 9.9925 Å, and β = 109.166° [Fig. 1(a)]. On the (-101) natural cleavage plane [Fig. 1(b)], there are two-leg ladders with two FeTe chains parallel to the short axis b, which are separated by a Ta/Te network in-between. Therefore, $TaFe_{1.23}Te_3$ possesses a quasi-one-dimensional crystal structure. Fig. 1(c) illustrates the three-dimensional Brillouin zone (BZ), and the corresponding surface BZ. We define the k_x and k_y axes to be parallel and perpendicular to the ladder/chain, respectively. The LEED pattern in Fig. 1(d) also manifests its twofold symmetry and confirms high sample quality.

The photoemission intensity map in Fig. 2(a) indicates two Fermi surface sheets. The periodic undulation-like Fermi surface along $\bar{\Gamma}\bar{Y}$ suggests sizable in-plane inter-ladder interactions. Figure 2(b) plots the momentum distribution curves (MDC's) along $\bar{\Gamma}\bar{X}$, and two bands α and α' could be observed near E_F. The Fermi surface of α' seems to have the same shape as that of α, but judging from their dispersions, α' is not a folded band of α. Moreover, the negligible photon energy dependence [Fig. 2(a), 2(c) and 2(d)] demonstrates the weak inter-plane coupling or quasi 2D nature of $TaFe_{1.23}Te_3$.

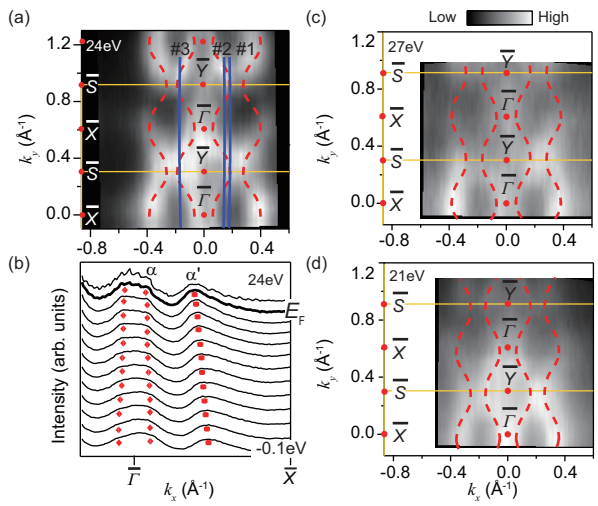

Fig. 2. (Color online). The Fermi surface of $TaFe_{1.23}Te_3$. (a) Photoemission intensity maps integrated within 10 meV around Fermi energy (E_F) with 24 eV photons at 30 K. (b) Momentum distribution curves (MDC's) near E_F along $\bar{\Gamma}\bar{X}$. Marks are guide to eyes of the dispersions. (c) and (d) Photoemission intensity maps integrated within 10 meV around E_F taken with 27, and 21 eV photons, respectively. The red dashed lines are the guides to eyes for the Fermi surface, which show weak k_z dependence. Data were taken with horizontally polarized photons at 13 K at UVSOR.

Three more bands β, γ, and δ can be identified along $\bar{\Gamma}\bar{X}$ (along the ladder) [Fig. 3(a) and 3(b)]. The β and γ bands disperse from 0.3 to 0.7 eV below E_F, while δ shows a parabola-like dispersion with a larger bandwidth. Along $\bar{\Gamma}\bar{Y}$ (perpendicular to the ladder), one could only observe the β, γ, and δ bands [Fig. 3(d) and 3(e)]. Along #1-#3 which are off the $\bar{\Gamma}\bar{Y}$ direction, dispersions of band α perpendicular to the ladder can be resolved [Fig. 3(g)-3(i)]. By fitting the dispersions by E=E_0+2$t$cos($\bar{b}k_{\parallel}$) [Fig. 3(g)-3(i)], we can extract the interladder hopping integral t, which is 0.054 eV for band α. We note that for FeTe, in the nonmagnetic state, the features are very broad, and the quasiparticle peak is undistinguishable even at E_F. However, in its bicollinear AFM state, when the magnetic fluctuations are gapped out, coherent quasiparticles show up.[13,14] Sharp quasi-particle peak is not observed in the AFM states of $TaFe_{1.23}Te_3$, which may be attributed to the strong and ungapped magnetic fluctuations in ladders.

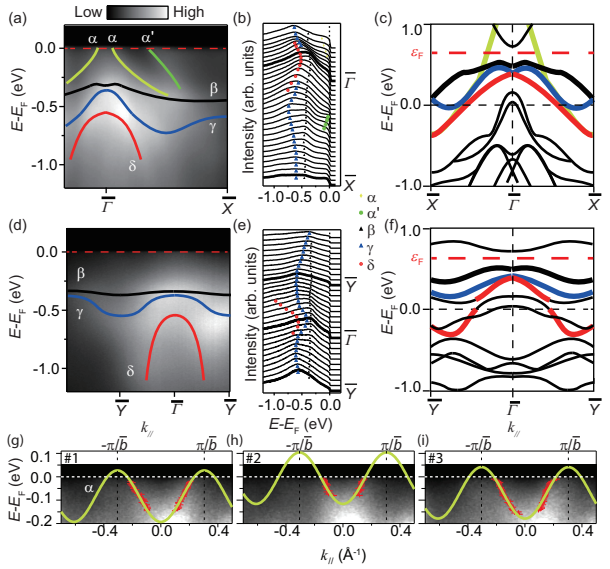

Fig. 3. (Color online). Band structure of $TaFe_{1.23}Te_3$. (a) Photoemission intensity along $\bar{\Gamma}\bar{X}$. (b) Plot of energy distribution curves (EDC's) along $\bar{\Gamma}\bar{X}$ in panel (a). (c) The calculated band structure along $\bar{\Gamma}\bar{X}$ without interstitial iron atoms Fe_2, the thickened part of the bands have been observed in our data. (d)-(f) are the same as panels (a)-(c), but for data along $\bar{\Gamma}\bar{Y}$. Marks are guide to eyes of the band dispersion which are determined by the local maxima of the EDC's. (g)-(i) Photoemission intensity along #1 - #3, respectively. The momentum locations are shown in Fig.2(a). The red markers show the experimental dispersions which are determined by the local maxima of the MDC's. The green curves show the fittings of the dispersions by $E{=}E_0{+}2t\cos(\bar{b}k_{||})$, where $\bar{b}$ is the surface lattice constant perpendicular to the ladder, and t is the interladder hopping integral. Data in panels (a),(b),(g),(h) and (i) were taken with horizontally polarized 24 eV photons at 13 K at UVSOR. Data in panels (d) and (e) were taken with circularly polarized 24 eV photons at 10 K at SLS. The red dashed lines in panels (c) and (f) indicate where the experimental Fermi energy is situated.

We calculated the band structure of $TaFeTe_3$ in the non-magnetic state without the interstitial Fe2 atoms. The calculation is conducted using the WIEN2K implementation of the full potential linearized augmented plane wave method in the local density approximation.[15] The k-point mesh was taken to be 4×5×11. The lattice constants were taken from ref. [16]. To compare with the APRES spectra directly, the band structure in 2-Fe zone is unfolded to the 1-Fe zone by applying the recent developed unfolding method.[17] Figures 3(c) and 3(f) exhibit the corresponding calculated band dispersions along $\bar{\Gamma}\bar{X}$ and $\bar{\Gamma}\bar{Y}$, respectively. The thickened part of the bands in the calculation are likely the bands observed in the experiment. The calculations partial qualitatively agree with the experiments, when considering some moderate band renormalization and the Fermi level shift due to the interstitial iron atoms in the real material (shown by the thick dashed lines). Note that the α' band is absent in our calculations, and its origin is still mysterious. There are several discrepancies between the experiment and the calculations, which demands further investigations, such as scanning tunneling microsope or transmission electron microscope studies on the roles of interstitial irons.

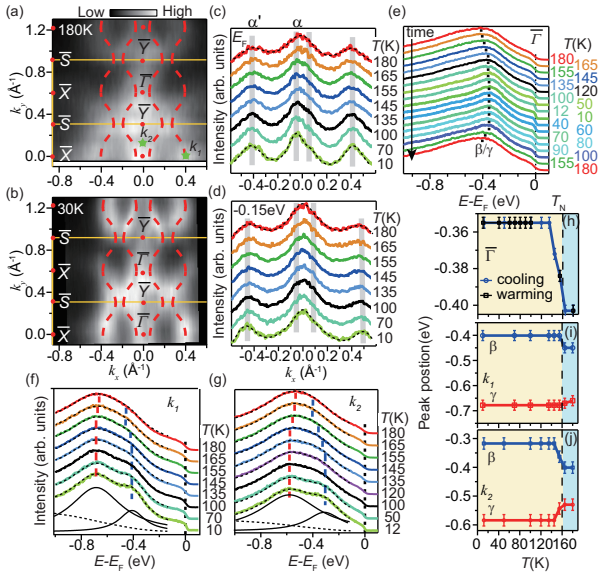

Fig. 4. (Color online). The temperature dependence of the electronic structure of $TaFe_{1.23}Te_3$. (a) and (b) Photoemission intensity map integrated within 10 meV around E_F, in paramagnetic (180 K) and antiferromagnetic (30 K) states, respectively. (c) Temperature dependence of MDC's at E_F along $\bar{\Gamma}\bar{X}$. (d) is the same as panel (c) but for data chosen at 0.15 eV below E_F. The black dash lines in panels (c) and (d) are the fitting curves at the lowest and highest temperatures to show the temperature independent peak positions. (e) Temperature cycling data of EDC's at $\bar{\Gamma}$. The bars illustrate the peak positions of the EDC's. (f) Temperature dependence of EDC's at a selected momentum k_1 marked in panel (a). (g) is the same as panel (f) but for data at k_2 marked in panel (a). In panels (f) and (g), examples of the fitted curve, Shirley background and Lorentzian are shown with thick dashed lines, thin dashed lines and solid lines, respectively. (h)-(j) The summary of the fitted peak positions of the EDC's in panels (e)-(g), respectively. The data in panels (a) and (b) were taken with horizontally polarized 24 eV photons at UVSOR. The data in panels (c)-(j) were taken with circularly polarized 24 eV photons at HSRC.

In the paramagnetic state [Fig. 4(a)] and AFM state [Fig. 4(b)], the Fermi surface intensity maps exhibit negligible change within the experimental uncertainty except some thermal broadening, and there is no AFM gap at the Fermi surface. The temperature dependence of the MDC's along $\bar{\Gamma}\bar{X}$ also show negligible movements of α and α' [Fig.4(c) and 4(d)], suggesting the AFM transition is not driven by the Fermi surface instability, although the AFM coupling is out-of-plane, the nesting condition would be fullfilled due to the weak k_z dependence. However, the β and γ bands shift towards lower binding energy as temperature decreases and shift back again without hysteresis when warming up [Fig.4(e)], indicating the second or-

der nature of the transition. Figures 4(f) and 4(g) display the spectra at two representative momenta k_1 and k_2 as marked in Fig. 4(a), at temperatures across the AFM transition. The peak positions as a function of temperature are summarized in Figs.4(h)-4(j). The shifts of their peak positions all begin around the bulk $T_{\rm N}$, and saturate quickly below 145 K.[1] Since the structural transition at $T_{\rm N}$ in $TaFe_{1.23}Te_3$ is absent, such an intrinsic electronic structure reconstruction should be related to the AFM transition. The shift is about +50 meV for β and -18 meV for γ at k_1, and +80 meV for β and -50 meV for γ at k_2, in quantity. They are comparable with the $k_B T_{\rm N}$ energy scale and those band shifts observed in the parent compounds of the iron-based superconductors.[9,11] We note that the upward shifts are larger than the downward shifts, and it seems the electronic energy is not reduced in the AFM state, different from the observations made in 2D iron pnictides [8,9] and FeTe [13]. Presumably, the bands would shift towards higher binding energy to reduce energy, however, further studies are needed to fully understand this issue.

Previous ARPES results of iron pnictides [9,11,18] and FeSe/$SrTiO_3$ thin films [19] show that electronic structure reconstruction rather than Fermi surface nesting drives the AFM transition. Theoretical studies on iron-based superconductors suggest that the Hund's rule coupling is a key factor for the correlations and local moments.[20−22] The recent transport measurement on detwined FeTe suggests that Hund's rule coupling dominates magnetism in FeTe.[23] For FeTe, the system is largely characterized by a polaronic electronic structure,[13,14] and the bicollinear antiferromagnetic transition there corresponds to large energy (∼0.6 eV) and momentum (over the entire BZ) scale spectral weight transfer. For $TaFe_{1.23}Te_3$, its large local moment of 2 μ_B/Fe is comparable to that of FeTe.[7] The difference is that $TaFe_{1.23}Te_3$ possesses 2D Fermi surface and significant in-plane dispersions. Therefore, the key electronic character here is the coexisting of itinerant and localized $3d$ states, and Hund's rule coupling between them is the main source of electronic correlation, just like in the iron based superconductors. In analogy to the double-exchange ferromagnetism observed in the manganites, the Hund's rule coupling here would introduce similar effects. This gives a naturally interpretation of the magnetic order in $TaFe_{1.23}Te_3$, as the in-plane magnetic order is determined by the competition between double exchange ferromagnetism and superexchange antiferromagnetism.[21] The chain-like structure of $TaFe_{1.23}Te_3$ significantly blocks the inter-chain superexchange between the in-plane localized spins as they are too far away, while the inter-chain hoppings of the itinerant electrons can still be mediated by the intermediate Ta (nonmagnetic $5d^1$) structure. Therefore, the in-plane FM coupling wins over the AFM one, resulting in the in-plane FM order shown in Fig. 1(b). On the other hand, the intra-ladder Fe-Fe or Fe-Te-Fe structure and the distance between planes [Fig. 1(a)] are similar to that of FeTe, and the direct FM exchange within a ladder and the inter-plane AFM superexchange may work similarly as in FeTe. Therefore, these conspire the so called A-type AFM order in $TaFe_{1.23}Te_3$.

To summarize, the quasi-two-dimensional Fermi surface and band structure were observed for $TaFe_{1.23}Te_3$, which is in a partial and qualitative agreement with the band calculations. Our results suggest that $TaFe_{1.23}Te_3$ is the second kind of novel quantum materials besides the parent compounds of iron-based superconductors, whose AFM transition directly correlates with the electronic structure reconstruction at high binding energies. The commonalities among $TaFe_{1.23}Te_3$, FeTe, and other parent compounds of iron-based superconductors suggest that they are just the different manifestations out of the competition among the same set of physical ingredients, such as the Hund's rule coupling and antiferromagnetic superexchange interactions between localized spins.[21] Particularly, this spin ladder system would provide a simpler testing ground to study the essence of magnetism in iron pnictides and chalcogenides.

We are grateful to Professor Jiangping Hu and Professor Hua Wu for helpful discussions.

References

[1] Liu R H et al 2011 *Phys. Rev.* B **84** 184432
[2] Lei H et al 2011 *Phys. Rev.* B **84** 214511
[3] Caron J M et al 2011 *Phys. Rev.* B **84** 180409
[4] McCabe E E, Free D G and Evans J S O 2011 *Chem. Commun.* **47** 1261
[5] Li W et al 2012 arXiv: 1210.4619
[6] Ke X et al 2012 *Phys. Rev.* B **85** 214404
[7] Li S et al 2009 *Phys. Rev.* B **79** 054503
[8] Zhang Y et al 2012 *Phys. Rev.* B **85** 085121
[9] Yang L X et al 2009 *Phys. Rev. Lett.* **102** 107002
[10] Ge Q Q et al 2013 *Phys. Rev.* X **3** 011020
[11] Yi M et al 2012 *Proc. Natl. Acad. Sci.* **108** 6878
[12] Wang X F et al 2009 *Phys. Rev. Lett.* **102** 117005
[13] Zhang Y et al 2010 *Phys. Rev.* B **82** 165113
[14] Liu Z K et al 2013 *Phys. Rev. Lett.* **110** 037003
[15] Schwarz K, Blaha P and Madsen G K H 2002 *Comput. Phys. Commun.* **147** 71
[16] Liu S X, Cai G L and Huang J L 1993 *Acta Crystallogr. Sect.* C **49** 4
[17] Ku W, Berlijn Tom and Lee Chi-Cheng 2010 *Phys. Rev. Lett.* **104** 216401
[18] He C et al 2010 *Phys. Rev. Lett.* **105** 117002
[19] Tan S Y et al 2013 *Nature Materials* **12** 634640
[20] Haule K and Kotliar G 2009 *New J. Phys.* **11** 025021
[21] Yin W-G, Lee C C and Ku W 2010 *Phys. Rev. Lett.* **105** 107004; Yin W-G, Lin C-H and Ku W 2012 *Phys. Rev.* B **86** 081106(R)
[22] Ong T Tzen and Coleman Piers 2012 *Phys. Rev. Lett.* **108** 107201
[23] Jiang J et al 2013 *Phys. Rev.* B **88** 115130